Influence of the porous transport layer properties on the mass and charge transfer in a segmented PEM electrolyzer

Julian Parra-Restrepo, Rémi Bligny, Jérôme Dillet, Sophie Didierjean, Didier Stemmelen, Christian Moyne, Alain Degiovanni, Gaël Maranzana

Influence of the porous transport layer properties on the mass and charge transfer in a segmented PEM electrolyzer

Julian Parra-Restrepo[a,b,*], Rémi Bligny[a], Jérôme Dillet[a], Sophie Didierjean[a], Didier Stemmelen[a], Christian Moyne[a], Alain Degiovanni[a], Gaël Maranzana[a]

[a]Laboratory of Energetics and of Theoretical and Applied Mechanics, University of Lorraine, 54500 Vandœuvre-lès-Nancy, France

[b]French Environment and Energy Management Agency ADEME, 49000 Angers, France

* *Corresponding author: parrares1@univ-lorraine.fr*

Abstract

A titanium Porous Transport Layer (PTL) is usually used at the anode side of PEM water electrolyzers to ensure both the gas/water transport and the electric charges transfer. In this paper, four different sintered Ti powder PTLs were characterized to determine some properties, such as the pore size distribution, the porosity, and the permeability. Their influence on the electrolysis performance was investigated by using a 30 cm^2 segmented cell which allowed measuring the current density distribution, while controlling temperature and pressure conditions. For a better understanding, in-situ techniques such as the Polarization Curves and the Electrochemical Impedance Spectroscopy (EIS) were used. A local characterization of mass transport limitations caused by oxygen saturation was carried out, paying special attention to the pressure influence when using a PTL with very small pores. The results showed that current density heterogeneities can be explained by microstructure changes along the PTL. The optimal geometric characteristics of the PTL depend not only on the operating conditions such as current density, pressure, and temperature but also on the catalyst layer properties. A new model for the constriction resistance between the catalyst layer and the PTL was proposed.

Keywords

PEM Electrolysis; Porous Transport Layer; Segmented electrolyzer; Mass transport limitations

1. Introduction

One of the main challenges of today is the energy transition, that is, the implementation of renewable energies to reduce our dependence on other energy sources that are highly harmful to the environment. The International Energy Agency (EIA) predicts that 30% of the electricity will be produced from "non-polluting" renewable sources by 2023 [1]. Nevertheless, the intermittency of some renewable sources (wind and solar) is a problem for the administration of the electrical grid since the energy production can be hardly predictable and therefore the electricity must be consumed immediately. In order to increase the participation of these clean sources in the energy mix, it is necessary to develop grid-scale storage means, which can both ensure energy supply during periods when the wind and the sun are absent, and allow adding value to the energy surpluses for other applications.

Water electrolysis is among the most promising solutions to this problem since it allows producing hydrogen, thus storing large amounts of energy for long periods. The produced hydrogen can then be used in Fuel Cells for transport and stationary applications to regenerate electricity, or it can be injected into the natural gas network to increase its calorific value. It can also be used for several industrial applications, e.g. the synthesis of ammonia, a fundamental element for fertilizer, or in the production process of float glass, used in car windshields and solar panels.

Large-scale water electrolysis would reduce the utilization of other hydrogen production methods, such as the coal gasification, the steam reforming of methane and the partial oxidation of hydrocarbons, that rely on fossil fuels and involve carbon emissions. In fact, up to 10 kg of CO_2 are generally released for each kilogram of produced hydrogen [2].

Alkaline and Proton Exchange Membrane (PEM) are the two technologies most widely used for the electrolysis of water. In contrast with alkaline electrolyzers, PEM electrolyzers can operate at higher current density, above 2 A cm^{-2}, which allows decreasing the footprint of the plant. Furthermore, these devices can directly deliver compressed hydrogen thanks to the polymer electrolyte membrane, and their transient response is in the range of 50ms [3], which is a major advantage when working with intermittent input power. This makes the PEM electrolyzers the most suitable devices for a direct connection with renewable energy sources [4–6]. However, larger PEM electrolyzers have to be developed to reach the aforementioned grid-scale energy storage capacity, and for this purpose, different problems limiting the performance must be solved [7]. Indeed, PEM electrolyzers are commonly affected by mass transport losses at the anode side, which cause the decrease of the efficiency [8].

It has been demonstrated that in the range of 1 A cm^{-2} to 2 A cm^{-2}, the mass transport losses account for 20-25% of the total losses, whereas the ohmic losses contribute with 20-30% of the total overpotential [9]. The key component responsible for these aspects is the Porous Transport Layer (PTL) used at the anode side of the electrolysis cell between the Membrane Electrode Assembly (MEA) and the bipolar plate, whose main purpose is both the transport of mass and the transfer of electric charges.

Regarding the mass transport, the PTL has to transfer the liquid water by capillarity from the bipolar plate channels to the catalyst layer, and simultaneously, has to remove the produced oxygen, resulting in a countercurrent two-phase flow through the porous medium. The improper evacuation of oxygen, and its accumulation in both the PTL and the electrode pores, can seriously decrease the performance of the PEM electrolyzer. Once the oxygen saturation occurs, the transport of water through the PTL is hindered. As a consequence, the membrane dehydration arises, and the Oxygen Evolution Reaction (OER) is affected. Moreover, the oxygen saturation can also affect the cooling of the electrolysis cell since the thermal conductivity of oxygen is lower than that of liquid water [10].

Additionally, regarding the transfer of charges, the PTL has to ensure an efficient electric contact between the catalytic layer and the bipolar plate, allowing the electrons transfer to the cathode side where they combine with protons producing hydrogen. Additional ohmic losses can arise if the contact between these elements is made incorrectly, producing heterogeneities in the current density distribution. This non-homogeneous current density distribution can generate “hot spots” when occurring along with the above-mentioned oxygen saturation of the PTL, which can either degrade the membrane or even destroy it when operating at high current density, as observed by Millet et al. [11,12].

There is a direct connection between the current density distribution and the gas/water transport limitations, especially the oxygen saturation in the PTL. The heterogeneous nature of these two phenomena indicates that they can appear on localized zones of the electrolysis cell. Hence, a segmented electrolyzer can be useful to make an accurate characterization.

In order to get the best performance, it is necessary to use a PTL with optimal characteristics that ensure an equilibrium between the transport of gas/water and the electric charges. Thus, the characteristics to be optimized are both the porosity and the pore size. Indeed, the porosity has a direct effect on the contact resistance between the MEA and the PTL [13]. A small porosity increases the contact surface but hinders the oxygen expelling. On the other hand, for a given porosity, large pores facilitate gas/water transport but will increase the electrical resistance since contact points (forming the contact surface) are more distant from each other. Conversely, small pores will improve

the electrical contact but gas expelling and the water feeding will be obstructed, increasing the mass transport losses [7].

In order to find this equilibrium, some authors have studied the influence of different PTLs on the efficiency of PEM electrolyzers, analyzing parameters such as pore size, porosity, thickness, and the size of particles or fibers for porous media in the form of sintered powder or felt. However, these works focused exclusively on the effects in the electrolysis cells from a global point of view, without paying attention to the local problems. Grigoriev et al. [14] prepared different PTLs using sintered and spherically shaped titanium powders. They found that the optimum particle diameter is between 50 and 75 μm, whereas the optimum mean pore diameter is 13-12 μm. They also showed that the use of an inadequate PTL could increase the overpotential up to 100 mV at 2 A cm^{-2} and atmospheric pressure. Majasan et al. [15,16] made an ex-situ characterization of four different PTLs with a mean pore diameter of 16 μm, 40 μm, 60 μm and 90 μm. They compared microstructure properties with the results obtained by electrochemical characterization of a PEM electrolyzer, finding a better performance for PTLs with small pores. Using Electrochemical Impedance Spectroscopy, the authors suggested that this result was due to an improvement in the electric contact between the PTL and the catalyst layer.

Siracusano et al. [17] studied the influence of the PTL thickness on the performance of a PEM electrolyzer using two grids of 260 μm and 500 μm, finding a better electric contact with the thicker grid. This differs from the results of Hua Li et al. [18] who compared several grids with a thickness of 200 μm and 300 μm. Ito et al. [19,20] also studied the influence of mean pore diameter but using titanium felts. Pore diameters between 10.1 and 38.6 μm were compared, concluding that the electrolysis performance improves with decreasing pore diameter within this range. The authors also concluded that changes in porosity have no significant effects on the performance of a PEM electrolyzer. Schuler at al. [21,22] compared a matrix of six PTLs with 2 porosities (56 % and 76%), three fiber diameters (11 μm, 15 μm, and 30 μm) and pore diameters between 17 μm and 124 μm. They focused on the electrical resistance between the catalytic layer and the PTLs and measured values between 9 mΩ cm^2 and 102 mΩ cm^2. The lowest resistance was measured for a PTL with a porosity of 56% and fiber diameter of 11 μm, and the highest one was measured for a PTL with a porosity of 76% and fiber diameter of 50 μm. Some studies have also addressed the mass transport problems inside the PTL from modeling point of view [23–29].

Some authors have also proposed to make PTLs with a micro-porous layer (MPL) to improve the mass transport and the electrical contact with the catalyst layer[30–34]. Lettenmeier et al. added a MPL of titanium particles not bigger than 45 μm on a sintered PTL made of particles between 100-200 μm

(mean pore size 17 μm), which allowed to reduce the contact resistance of 20 mΩ cm^{-2}. In another publication, the authors proposed MPLs with a pore size gradient between 5 and 10 μm, finding that the optimal pore diameter in contact with catalyst layer is around 6 μm.

Only a few publications have reported the use of segmented electrolyzers [35–41]. These works focused on the influence of the stoichiometric feed water ratio on both the current density distribution and the thermal management of the electrolysis cell. Sun et al. [38] used a circular cell with both the anodic catalyst layer and the Ti-PTL segmented in 11 circles and regrouped them into 5 measurements zones between the inlet and outlet. They studied the behavior of the cell under water starvation conditions, and reported that the current density decreased along the 5 zones when the stoichiometric ratio was highly reduced (λ≤3). Nevertheless, no further information about the PTL was given. Immerz et al. [39] studied the influence of water flux on the performance of a PEM electrolyzer using a single channel cell with a surface area of 50.4 X 0.45 cm^2 divided into 252 segments of 2mm each. Two titanium felts were used as PTLs in both sides of the electrolyzers (thickness of 1 mm, porosity 0.5, fiber diameter of 20 μm). Their work showed that water flux reduction led to an increase of the overall potential whereas the current density distribution decreases between the inlet and the outlet of the cell, in full agreement with the work of Sun et al. [38].

This review shows that no study of the influence of the PTL using segmented electrolyzers has been made yet. In addition, there is a lack of knowledge about the local transport limitations and the uneven current distribution caused by oxygen saturation when operating at high current density and constant stoichiometry water feed ratio. Understanding these phenomena is essential for the optimization and design of large-scale PEM electrolyzers.

In the present work, we investigated the influence of sintered Ti-PTLs with different pore sizes on the local behavior of a PEM electrolyzer. For this purpose, we used a segmented cell which allowed measuring the current density distribution, while controlling temperature and pressure conditions. The performance of the PEM electrolyzer was analyzed by using in-situ techniques such as Polarization Curves and Electrochemical Impedance Spectroscopy (EIS). We also proposed a model of the constriction resistance in the catalyst layer that is affected by the geometric characteristics of the PTL. Moreover, a local characterization of mass transport limitations caused by oxygen saturation was made paying special attention to the pressure influence.

2. Experimental

2.1 Materials and experimental set-up

The electrolyzer used in the present work was a single 30 x 1 cm^2 cell that has already been described elsewhere [42,43]. The end plate of the anode side, which is made of titanium to resist the high potentials, has four parallel channels with a cross section of 0.15 x 0.15 cm^2 to supply the water and to expel the oxygen (Figure 1a).

The end plate of the cathode side is made of 316L stainless steel with a 1.5 µm gold coating that improves the electrical contact with the carbon gas diffusion layer, reducing the ohmic overpotential. The flow zone is divided into 20 electrically insulated segments that allow the current to be collected independently along the active area. Each segments measures 1.5 x 1 cm^2. A segmented reference electrode, through which humidified hydrogen flows, allows measuring the cathode potential and deducing the local anode potential between the inlet and the outlet of the cell. However, the results obtained with this reference electrode are not presented herein. An external power supply of nominal capacity 3300 W was used.

The used membrane-electrode assembly (MEA) was fabricated by Greenerity GmbH under the commercial name E300 (30 x 1 cm^2 active area and 150 µm thick). At the cathode, a gas diffusion layer (GDL) 420 µm thick, coated with microporous layer (MPL) and fabricated by SGL Carbon (SGL 10BB), was used. The in-plane conductivity of this GDL is low enough to allow a good measurement of the local current density. At the anode, sintered Titanium powder PTLs were used and they are described below.

The electrolyzer temperature was precisely set by a thermostatic bath driven by a platinum Pt100 probe inserted in the anode plate. Additionally, the presented experimental set-up allows increasing the relative pressure of both cathode and anode side up to 6 Bar (Figure 1b).

Preheated and de-ionized water were supplied to both sides of the electrolysis cell, to the anode side as the reactant, and to the cathode side to ensure a good thermal homogeneity. The feeding water temperature was measured at the inlet and outlet of both compartments.

An ion-exchange resin, provided by Dow Chemical under the commercial name of AMBERLITE™ IR120H, was used in order to keep the water resistivity above 16 MΩ. Two micro annular gear pumps mzr-7265 were used to ensure constant low flow rates (0.048 – 288 ml min^{-1})

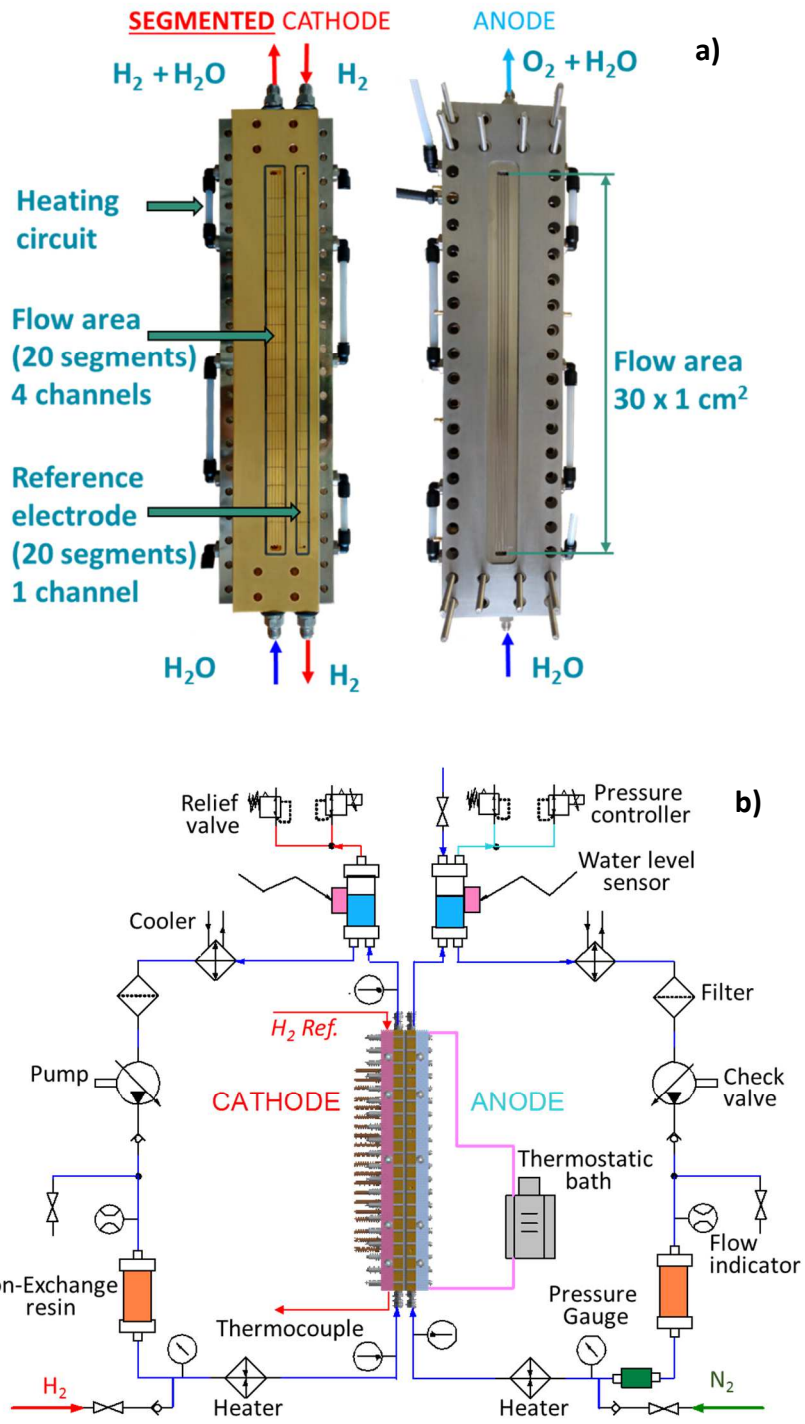

Figure 1. Segmented electrolysis cell : Cathode (Brass + Nickel and Gold plating) and Anode (Titanium). (b) Test bench

2.2 Porous Transport Layer (PTL)

Four PTLs with different pore diameters and a thickness of 1 mm were tested in the anode side of the electrolysis cell. These PTLs were fabricated from sintered Titanium powder and they were characterized by using the Mercury Intrusion Porosimetry (MIP) technique to obtain the pore diameter distribution and the porosity. The device used for the characterization was the AutoPore IV

9500 V1.09, which was provided by Micromeritics and has a pressure range going from 0.0035 MPa to 219 MPa.

2.3 Electrochemical characterization

An experimental protocol for the MEA conditioning was performed to startup the electrolyzer. It consists of a cycle in which polarization curves are measured, first at 60°C and then at 80°C, while the system pressure is progressively increased from atmospheric pressure to 6 bar for each temperature. This cycle was repeated twice and lasted two days. Such a protocol was established in order to ensure the reliability of the results presented herein, since the behavior of the electrolyzer was found to change drastically during the first hours of operation, which was attributed to the conditioning of the MEA.

In order to record the polarization curves, the current density of the cell was changed stepwise between 0.1 A cm^{-2} and 3.3 A cm^{-2} in one up-and-down cycle. Each current density was held for 4 minutes to allow the voltage response stabilizing, but only the last 120 seconds of each stage were taken into account to calculate the average potential. Since an up-and-down technique was used, two curves were recorded, one when increasing the current density and the other when decreasing it. The water stoichiometry was kept equal to 50 for each measurement.

3. Results and discussion

3.1 PTL characterization

The pore size and the porosity of each PTL were first measured since the main purpose of this work is to investigate how they affect the performance of the electrolysis cell. Figure 2 shows the pore size distributions obtained with the mercury intrusion technique. A unimodal distribution was obtained for all the PTLs. PTL-VS (Figure 2a) exhibited a narrow peak around 2-3 µm, whereas a peak at 10 µm was observed for PTL-S (Figure 2b). On the other hand, a larger dispersion was obtained for the PTL with larger pores. Specifically, a broad peak at 35 µm was obtained for PTL-M (Figure 2c), whereas a broader one was measured for PLT-L and centered at 60 µm (Figure 2d).

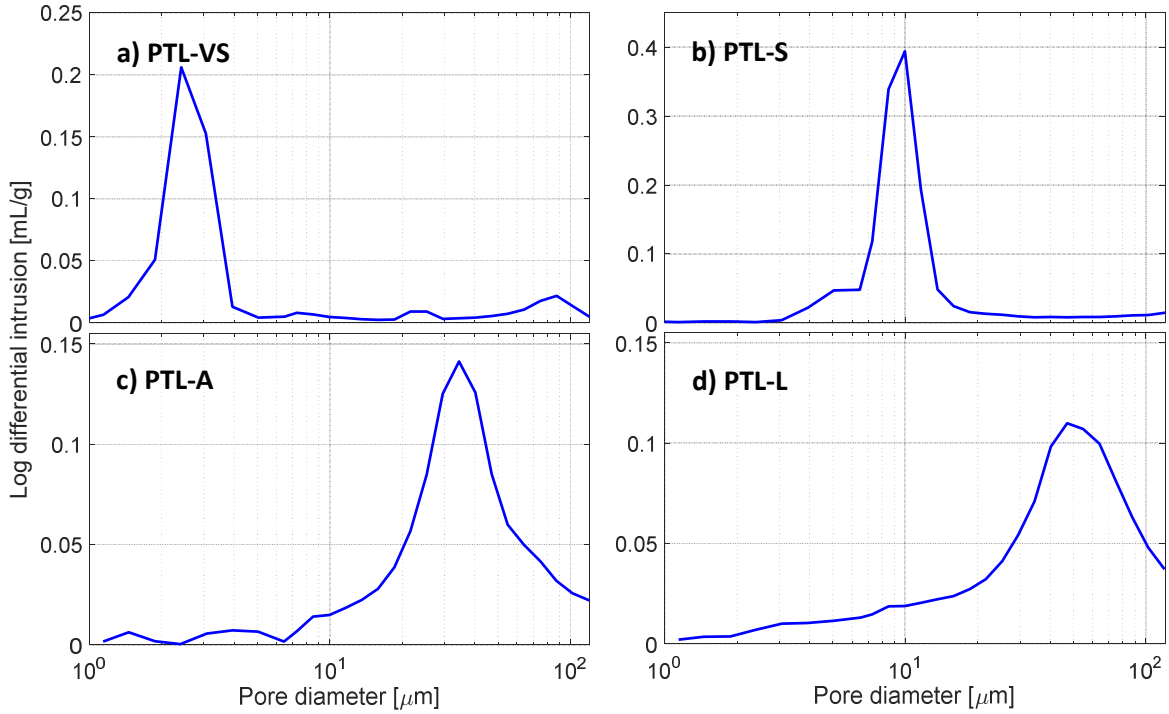

Figure 2. Pore size distribution obtained with the mercury intrusion technique

Table 1 summarizes the measured values of the mean pore size and the porosity as well as the name assigned to each PTL. Porosity was found to increase with the pore size, although these two parameters are independent of each other. Nevertheless, they do not increase in the same proportion. For instance, between PTL-S and PTL-L, the mean pore size is 6 times higher, whereas the porosity increases by only 6%. Thus, the pore size should have more effects herein.

	Mean pore size D_p (µm)	***Porosity (%)***
PTL-L (Large)	60 ± 1.5	37
PTL-M (Medium)	35 ± 1.5	34
PTL-S (Small)	10 ± 1.5	31
PTL-VS (Very Small)	3 ± 1.5	26

Table 1. Mercury Intrusion Porosimetry (MIP) results.

3.2 I-V curves

The cell was assembled with the PTL-S, PTL-M and PTL-L. The polarization curves obtained from the up-and-down cycle described in Section 2.3 are shown in Figure 3 for a working temperature of 60°C and atmospheric pressure.

A linear increase of the cell voltage with the current densities higher than 0.5 A cm^{-2} was observed for the three mentioned PTLs. This means that, no apparent mass transport limitations were detected in the whole range of measured current densities, hence the increase in the ohmic losses had a predominant role herein. Nevertheless, two different regions of interests can be identified where the relative position of the polarization curves for three PTLs changed:

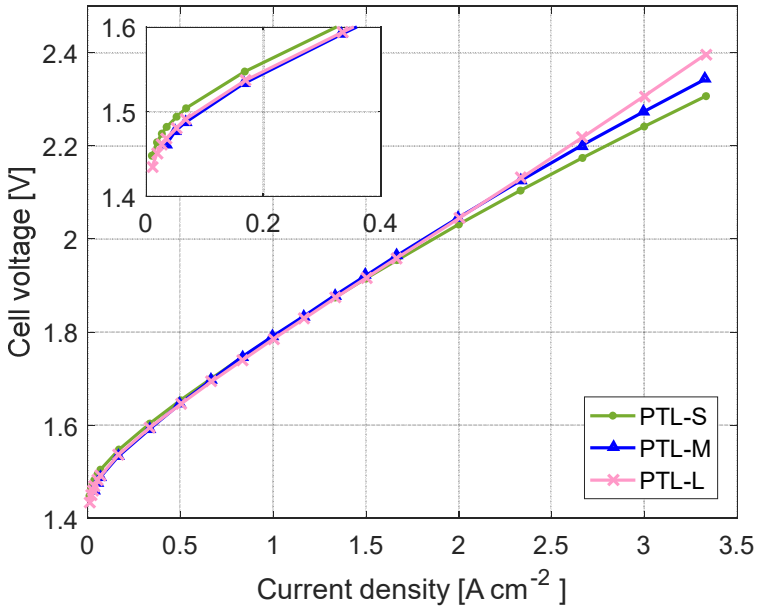

Figure 3. Average polarization curves of the up-and-down cycle for PTL-S, PTL-M and PTL-L at 60 °C and atmospheric pressure.

1) At low current densities (i ≤ 0.5 A cm^{-2}), the voltage is slightly higher when using a PTL with small pores instead of one with large pores. This can be explained by the variation of the Nernst potential due to the increase of the gas pressure inside the electrode as the gas must repel the liquid water to be expelled. As a first approximation, the gas pressure in the electrode has the same order of magnitude as the sum of the capillary pressure and the liquid pressure. Assuming that the liquid pressure is nearly uniform in the PTL and that the pores are similar to capillary tubes, the capillary pressure can be calculated using the Laplace's Law:

$$P_{cap} = \frac{2\gamma\, cos\theta}{R_p} \qquad (1)$$

Where γ [N m^{-1}] is the surface tension, R_p [m] is the pore radius and θ is the contact angle that can be considered equal to zero to give an order of magnitude of the pressure. According to the Laplace's Law, the smaller the pore size the higher the capillary pressure. For example, a pore size of 3 µm leads to a capillary pressure of 0.5 bar, whereas a pore size of 60 µm leads to a capillary pressure of 0.25 bar. The corresponding Nernst potential variations can be calculated as follows:

$$\Delta E(3\mu m) = \frac{RT}{2F} ln\left(\sqrt{\frac{P_{atm} + P_{cap}(3\mu m)}{P_{atm}}}\right) = 3mV$$

$$\Delta E(60\mu m) = \frac{RT}{2F} ln\left(\sqrt{\frac{P_{atm} + P_{cap}(60\mu m)}{P_{atm}}}\right) = 0.2mV$$

In addition, the activation losses can also be affected since the exchange current density is a decreasing function of the oxygen pressure.

2) At high current densities, lower cell voltages were obtained when using the PTL with the smallest pores. For instance, at 3.3 A cm^{-2}, the cell voltage for PTL-S was about 100 mV lower than for PTL-L. Following the same trend, the polarization curve of PTL-M was found to be between the other two.

The reduction of the electrical resistance between the PTL-S and the catalyst layer, which is improved by small pore diameters and small porosities, may explain these voltage differences: the presence of small pores implies that the distance between contact points is shorter. Therefore, electrons must follow a shorter path through the catalyst layer plan to reach the PTL, as shown in Figure 4a. The opposite effect is obtained when the pores are larger, as in the case of the PTL-L. The number of contact points is reduced and they are more distant from each other. Thus, electrons must follow a longer path through the plane of the catalysts layer to reach the PTL, as shown in Figure 4b, making the contact resistance to increase.

Regarding the porosities, the surface contact area between PTL-L and the catalyst layer is slightly reduced since the porosity of the PTL-L is 6% larger than that of PTL-S.

In conclusion, the reduction of the contact surface area caused by the increase of the porosity as well as the larger distance between contact points caused by larger pores, ended up by increasing the cell voltage.

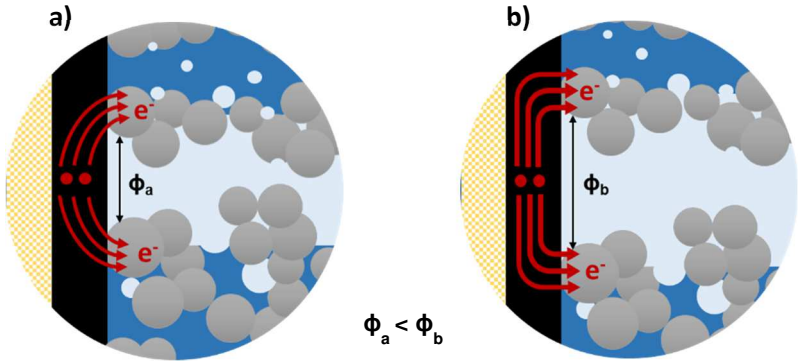

Figure 4. Transfer path of electric charges when changing the pore size. a) Small pores, b) large pores

The electrical resistance R_e between the catalytic layer and the PTL is the sum of three resistances:

$$R_e = R_{CL}^c + R_{PTL}^{TiO_2} + R_{PTL}^c \quad (2)$$

- R_{CL}^c is the resistance related to the path followed by electrons in the catalyst layer, and it is affected by the "geometric" characteristics of the PTL. It is called the "constriction resistance", and it depends on both the electrical conductivity σ [S m^{-1}] and the thickness of the catalyst layer *e* [m] as well as on the size of the PTL pores D_p [m], as explained above. The constriction resistance can be analytically derived for an axisymmetric geometry (Section 3.3).
- $R_{PTL}^{TiO_2}$ is the resistance of the thin semiconductor layer of titanium oxide that covers the PTL particles. It takes into account the contact area between the catalyst layer and the PTL and, therefore, it depends on the porosity of the PTL and on the clamping pressure. The thickness of titanium oxide may change depending on the operating conditions, mainly on the potential.
- R_{PTL}^c is the constriction resistance due to the path that electrons follow in the PTL. This resistance can be neglected due to the good electrical conductivity of titanium.

3.3 Constriction resistance:

In order to model the aforementioned constriction resistance R_{CL}^c [Ω cm^2], the catalyst layer was modeled as a porous medium formed by parallel cylinders of radius *R* [m] and height *e* [m], *e* representing the electrode thickness as shown in Figure 5. The bottom of the cylinders is in contact with the membrane and the top is contact with the PTL. The charges are transferred between the PTL and the catalyst layer through this surface that is given by a circle of radius *a* [m].

The pores diameter (D_p) and the porosity (ε) of the PTL can be deduced from Figure 5 as follows:

$$D_p = 2(R - a) \quad (3)$$

$$\varepsilon = 1 - \frac{a^2}{R^2} \quad (4)$$

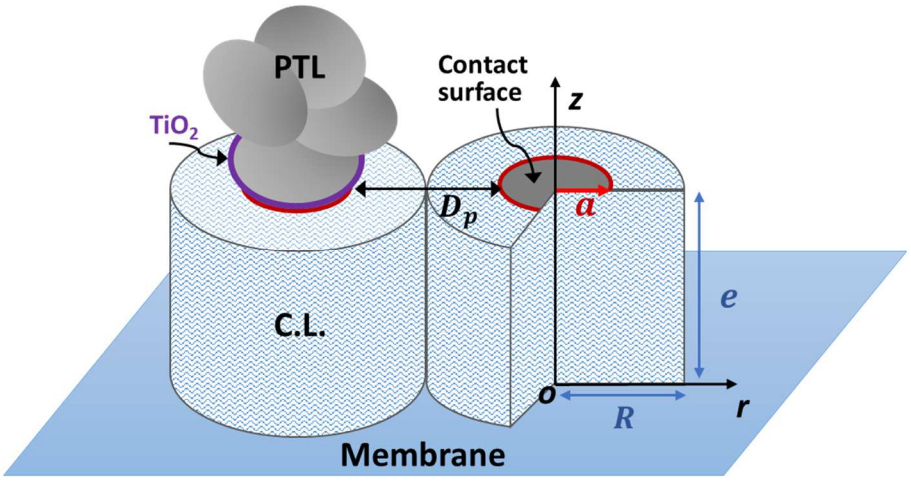

Figure 5. Representation of the contact between the PTL and the Catalyst Layer (C.L.). In order to get an analytical solution, a cylindrical catalyst layer is considered

The potential *V(r,z)* in the catalyst layer was calculated by using the local Ohm' law Eq (5) and the charge conservation Eq (6) at steady state:

$$\vec{\imath} = -\sigma \vec{\nabla} V \tag{5}$$

$$\vec{\nabla}.\vec{\imath} = p_0 \tag{6}$$

Where σ [S m^{-1}] is the electrical conductivity of the catalyst layer, and p_0 [A m^{-3}] is the volumetric source that is considered uniform in the catalyst layer. Combining both equation, the following differential equation is obtained Eq. (7):

$$\frac{\partial^2 V}{\partial r^2} + \frac{1}{r}\frac{\partial V}{\partial r} + \frac{\partial^2 V}{\partial z^2} + \frac{p_0}{\sigma} = 0 \tag{7}$$

Considering that, electric charges produced by the oxygen evolution reaction cannot be transferred through the membrane (*z=0*) and that they are only transferred towards the PTL (*z=e*) by crossing the electrode thickness, the boundary conditions of Eq. (7) can be fixed as follows:

$$\left.\frac{\partial V}{\partial z}\right|_{z=0} = 0 \qquad \left.\frac{\partial V}{\partial r}\right|_{r=0} = 0$$

$$-\sigma\left.\frac{\partial V}{\partial z}\right|_{z=e} = i_0(r) \qquad \left.\frac{\partial V}{\partial r}\right|_{r=R} = 0 \tag{8}$$

Where $i_0(r)$ [A m^{-2}] is the current density through the contact surface. After solving analytically the Eq. (7), the following expression was found for *V(r,z) :*

$$V(r,z) = A_0 + \sum_{n=1}^{\infty} A_n J_0(\alpha_n r)\cosh(\alpha_n z) - \frac{p_0 z^2}{2\sigma} \tag{9}$$

Where J_0 is the Bessel function of order "0" and $\omega_n = \alpha_n R$ are the roots of the Bessel function of order "1" ($J_1(\omega_n)$=0), which were obtained numerically. The value of A_0 is given by the first root of J_1, and A_n is found using the boundary conditions:

$$A_n = -\frac{1}{\sigma\alpha_n \sinh\left(\frac{\omega_n e}{R}\right)} \frac{p_0 R^2 e}{a^2} \frac{\frac{a}{\alpha_n} J_1(\omega_n a/R)}{\frac{R^2}{2} J_0^2(\omega_n)} \quad (10)$$

The constriction resistance was calculated using the following expression:

$$R_{CL}^c = \frac{< \bar{V} > - \bar{V}(z=e)}{I} \quad (11)$$

With $I = p_0 \pi R^2 e$ [A] as the total current. $\bar{V}(z=e)$ is the voltage surface averaging and $< \bar{V} >$ is volume averaging, which is used because the charge production was supposed uniform.

$$\bar{V}(z=e) = \frac{2}{a^2}\int_0^a V(r, z=e) r dr = A_0 + \sum_{n=1}^{\infty} A_n \cosh(\alpha_n e) \frac{2}{a\alpha_n} J_1(\alpha_n a) - \frac{p_0 e^2}{2\sigma} \quad (12)$$

$$< \bar{V} > = \frac{2}{eR^2}\int_0^e \int_0^R V(r,z) r dr dz = A_0 - \frac{p_0}{\sigma}\frac{e^2}{6} \quad (13)$$

Then, the expression of the constriction resistance between the PTL and the electrode was deduced:

$$R_{CL}^c = \frac{e}{3\sigma\pi R^2} + \frac{4R}{\pi\sigma a^2} \sum_{n=1}^{+\infty} \frac{J_1^2\left(\frac{\omega_n a}{R}\right) \cosh\left(\frac{\omega_n e}{R}\right)}{\omega_n^3 J_0^2(\omega_n) \sinh\left(\frac{\omega_n e}{R}\right)} \quad (14)$$

The first term of the R_{CL}^c expression is the 1D resistance of the catalyst layer, that is the electrical resistance when the transfer of electrons is parallel to the $\overrightarrow{oz}$ direction. The second term, which is expressed as an infinite sum, is the additional resistance caused by the constriction of the flux lines, *i.e.,* the 3D character of the electron transfer.

Conductivity of the anode catalyst layer (σ)	225 S m^{-1}
PTL porosity (ε)	37 %
High Frequency Resistance of the electrolyzer	200 mΩ cm^2

Table 2. Reference values for the estimation of the constriction resistance. The electronic conductivity was measured using the four probes method.

Figure 6 shows the evolution of the constriction resistance (R_{CL}^c) as a function of the pore size (D_p) for different catalyst layer thicknesses (e). These results were obtained using the parameters of Table 2, which were previously measured.

For a given value of e, the resistance increases exponentially with the pore diameter. As mentioned in section 3.2, this occurs because electrons must follow a longer path to reach the PTL since the

contact points are more distant between them. On the other hand, for a given pore diameter, the resistance increases as the catalyst layer thickness decreases. This occurs because the electrons must follow a tighter path inside a thinner catalyst layer.

Figure 6 also shows the high frequency resistance (HFR) of the electrolyzer used herein (horizontal line). Following the profile of *e*=10 µm, which is the thickness of the catalyst layer used to obtain the experimental results of this work, it can be seen that R_{CL}^{c} becomes important compared to the HFR for pore diameters larger than 150 µm, reaching a value of 10%.

From these results, it can be concluded that the optimal pore size of the PTL depends not only on the operating conditions (current density, pressure, temperature), but also on the thickness and the electrical conductivity of the catalyst layer. Thus, the optimization must be performed on both the catalyst layer and the PTL. For example, if the thickness of the catalyst layer is reduced to save catalyst, or if the electrical conductivity decreases due to the use of supported catalyst, then the pore size of the PTL should be reduced too.

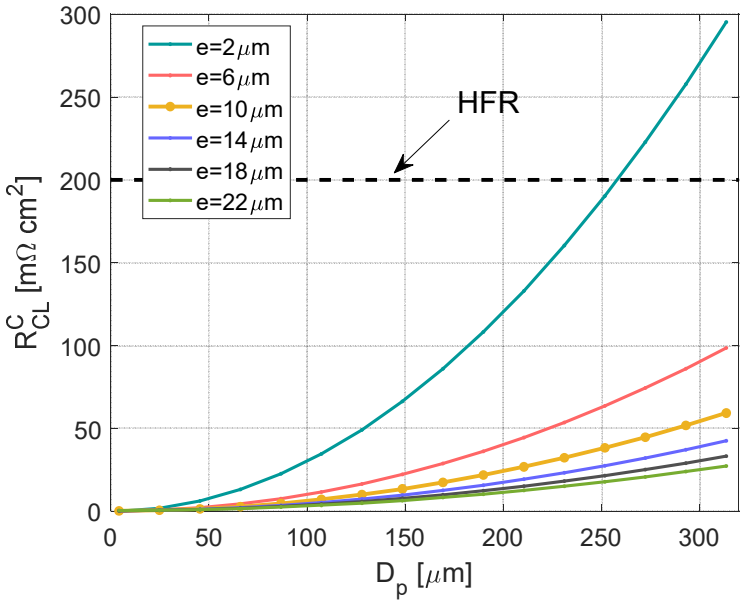

Figure 6. Evolution of the constriction resistance when changing the PTL pore size and the catalyst layer thickness

3.4 Transport limitations

The polarization curves for PTL-VS and PTL-S are presented in Figure 7. Only the ascending part of the up-and-down cycle was taken into account since a hysteresis phenomenon was observed between the PTL-VS curves. The increase in voltage was limited to a maximum of 3 V to limit the degradation of the cell components during the test.

The polarization curve measured in the case of PTL-VS was completely different from the other ones. The behavior was no longer linear as the cell voltage sharply increased when increasing the current density, highlighting the presence of transport limitations. This behavior can be explained through the electrode saturation by oxygen. Indeed, the oxygen production rate increases proportionally with the current density according to the Faraday's Law and produce a saturation at high current density, especially when PTLs with small pores are used. As a consequence, the water transfer from the flow channels towards the catalytic sites is hindered by the countercurrent flow of the evacuating oxygen, thereby preventing the OER reaction from occurring herein.

This phenomenon was sharpened around 1.85 A cm^{-2}, where the polarization curve became almost vertical. This point can be defined as the "limiting current density ", i_{lim}, and represents the maximum current that the reaction can provide. This means that the reaction cannot occur beyond this point because not enough water reaches the electrode.

The appearance of transport limitations means a great loss of efficiency. In addition, understanding this type of issue would play an important role both in the scaling up of the next generations of PEM water electrolyzer cells and in the increase of operating nominal current density.

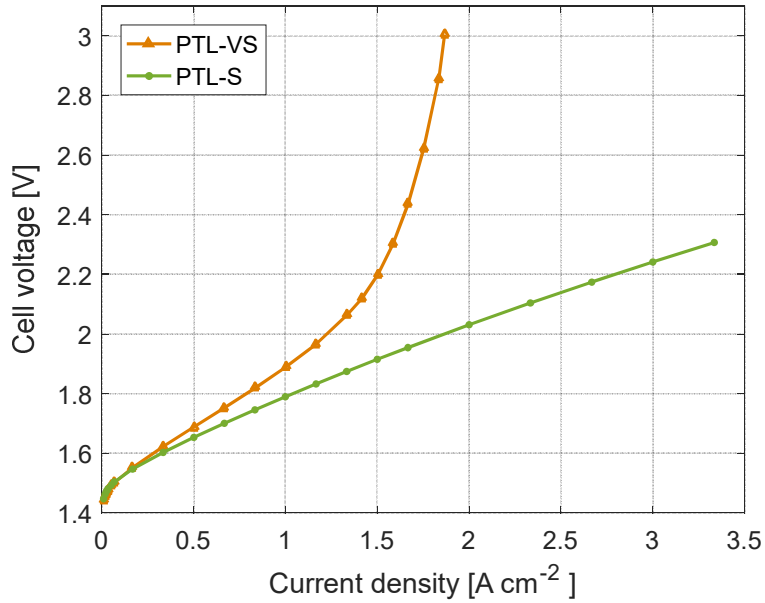

Figure 7. Polarization curve for PTL-VS : transport limitations evidence at 60 °C and atmospheric pressure

3.5 Hysteresis during the polarization curve in one up-and-down cycle

Figure 8 shows the two polarization curves obtained for the PTL-VS during the up-and-down cycle. This test highlighted the existence of a hysteresis effect between the two curves, the cell voltage of the descending curve being higher than that measured for the ascending curve. This can be explained

by both the process of imbibition and drainage in the PTL [44]. Drainage is the diffusion transport process of a nonwetting phase within a porous medium that displaces a wetting phase. If a continuous wetting phase is considered at the outset, it will become gradually disconnected in the process and part of it will be trapped. Therefore, the ascending curve can be associated to a drainage process since we assumed that the PTL was saturated in water before starting the measurement of this curve. Then, as the current density increased, the gas replaced the water until the limiting current density was reached, making the cell voltage increasing sharply. At this point, we assume that the PTL was mostly saturated with oxygen.

On the other hand, imbibition is the diffusion of a wetting phase within a porous medium that displaces a non-wetting phase. In this case, part of the non-wetting phase will be trapped, which will prevent the liquid from saturating all the pores. Thus, the descending curve can be associated to an imbibition process since the water began to saturate the PTL as the amount of oxygen gradually decreased.

However, when the process of drainage and imbibition are repeated consecutively, as it was for the curves in Figure 8, a saturation hysteresis appears [44]. This means that the state of water saturation that the PTL had just before drainage is not recovered after imbibition due to oxygen bubbles trapped inside. Thus, the water had more difficulty to reach the catalyst layer than in the initial state, which explains why the voltage of the descending curve was higher.

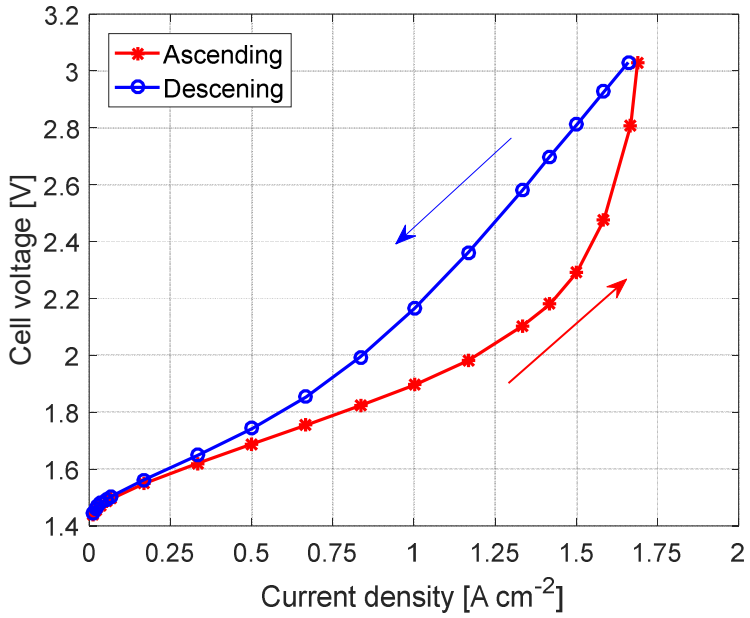

Figure 8 Polarization curve recorded during the up-and-down cycle at 60 °C and atmospheric pressure.

The time step applied to build polarization curve was too short to restore the water saturation state of the PTL-VS. This suggests that when high current densities are reached it is necessary to allow

more time to re-saturate the PTL with water and recover the performance. A more extensive analysis is ongoing, taking into account both the type of material used and the influence of operating conditions.

3.6 Operating pressure Influence

Figure 9a shows the polarization curves recorded when raising the pressure of both anode and cathode up to 6 bar. The same procedure used in Section 3.2 was used here, setting the temperature of the cell at 60°C and maintaining a water stoichiometry ratio of 50. Due to the hysteresis phenomenon described in Section 3.5 for PTL-VS, only the ascending curve of the up-and-down cycle were taken into account.

The recorded curves show that the operating pressure has a very important influence on the gas/water transport through the PTL, and it directly affects the voltage response of the electrolysis cell. At high current density (i > 1.5 A cm^{-2}), the cell voltage was found to be lower when increasing the pressure. For instance, at 1.75 A cm^{-2}, there was a remarkable reduction of 300 mV when the pressure went from the atmospheric pressure to 6 bar. The inverse behavior was observed at low current densities (i < 1.5 A cm^{-2}), i.e., the cell voltage was found to be higher when applying a higher operating pressure. For instance, at 0.5 A cm^{-2}, the voltage was found to be 40 mV higher when the cell operated at 6 bar instead of the atmospheric pressure. As previously described in Section 3.2, the pressure effect on the reaction thermodynamics described by the Nernst equation predominated at low current densities.

In the same way, the operating pressure had a significant impact on the limiting current density. Indeed, the limiting current density was 1.85 A cm^{-2} when the cell operated at atmospheric pressure, and it gradually shifted towards higher values when increasing the operating pressure, reaching the value of 2.27 A cm^{-2} for 6 bar. Thus, an increase of 22% was obtained by increasing the operating pressure of 6 bar.

The change of the limiting current density, as well as the reduction of the cell voltage for a given current density, is the result of the decrease of the volume of oxygen bubbles derived from the pressure increase. Then, the PTL saturation is reduced and the gas expelling is facilitated, leaving more space available for the water to reach the catalytic sites. Figure 9b shows that the limiting current density increases almost linearly with the operating pressure at 60°C and 80 °C.

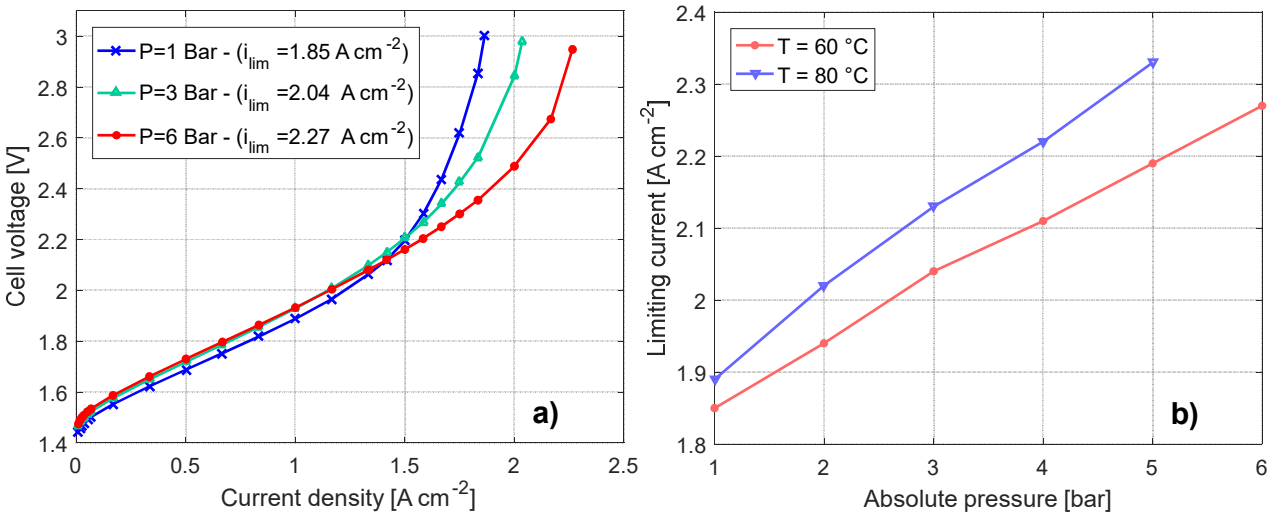

Figure 9 a) Polarization curves using the PTL-VS at 60 °C and b) Limiting current densities recorded for T=60 °C and 80 °C

Furthermore, for a given pressure, the limiting current density increases with temperature, which results in a larger working range for the electrolysis cell. Indeed, high temperatures improve the water transfer through the PTL as the liquid water viscosity is lower at these conditions, even if in the same time the gas flow increases because of the higher vapor saturation pressure and lower density.

3.7 Electrochemical Impedance Spectroscopy (EIS)

Electrochemical Impedance Spectroscopy (EIS) technique was used in order to analyze the behavior of the MEA face to the mass transfer limitations. The test was carried out at 1.5 A cm^{-2} with an amplitude of 10%, varying the frequency between 10 mHz and 10 kHz. The electrolysis cell was operated at 60°C, and a water stoichiometry of 50 was maintained.

Figure 10 shows the spectrum obtained by changing the pressure between the atmospheric pressure and 6 bar. The high frequency resistance (HFR) is associated with the electrical resistance of the entire electrolysis cell. Taking into account that all the tests were performed for the same assembly and for the same current conditions, we considered that the contact resistance between the metal components was kept constant, and therefore, only the variation of the conductivity of the membrane and ionomer affected the results.

A significant decrease of the HFR was observed when the pressure increased, resulting in a total reduction of 220 mΩ cm^2 over the entire tested pressure range. This reduction was explained by the improvement of membrane conductivity due to a better humidification at 6 bar.

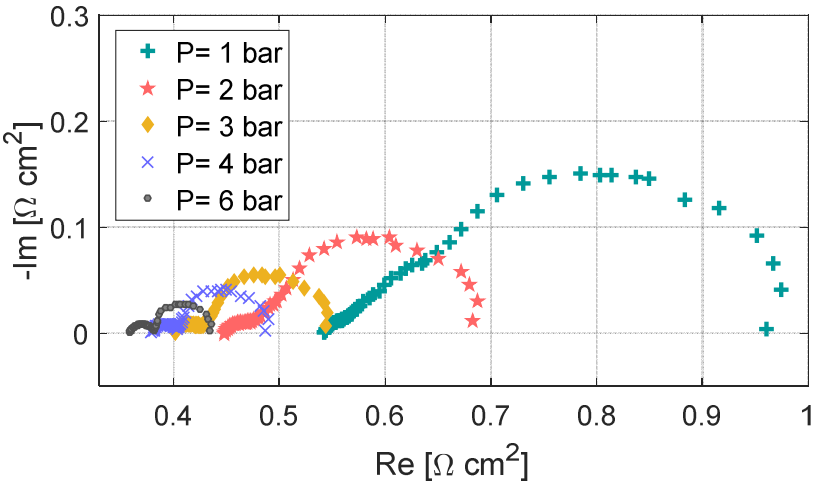

Figure 10. EIS results when increasing the pressure up to 6 bar at 60 °C

3.8 Local characterization of mass transport limitations

The local current density distribution was measured using the segmented electrolyzer. Two test were performed by changing the orientation of the PTL-VS. Then, the ends of the PTLs were named with the letters “m” and “n”.

Test 1 (orientation m-n):

For this test, the end “m” was placed at the inlet and the end “n” at the outlet of the electrolyzer. This orientation was the same used for the test presented in Section 3.4. The Figure 11a shows two current density profiles: the profile in black was recorded for a global current density of 1 A cm^{-2}, and the blue one was recorded when the global limiting current density was reached (1.85 A cm^{-2}) i.e. when the cell voltage sharply increased to reach 3V (Figure 7).

It can be seen that at 1 A cm^{-2} the profile was relatively flat along the electrolysis cell. However, the current distribution was heterogeneous when the mass transport limitations became predominant and the limiting current density was reached. It was found that the local current density remains around 1.5 A cm^{-2} in the inlet zone (Segments 1 to 6), whereas it is higher than 2 A cm^{-2} in the outlet zone.

This heterogeneous distribution appears more clearly on the local polarization curves of Segment 1 (inlet) and Segment 20 (outlet) that are presented in Figure 11b. In agreement with the current density profile, these curves show that transport limitations were more important in the inlet area than in the outlet one. It suggested that the transport of gas/water and electric charges through the PTL-VS was not homogeneous along the electrolysis cell.

A second test using the same PTL-VS was carried out in order to analyze its influence on the local transport limitations

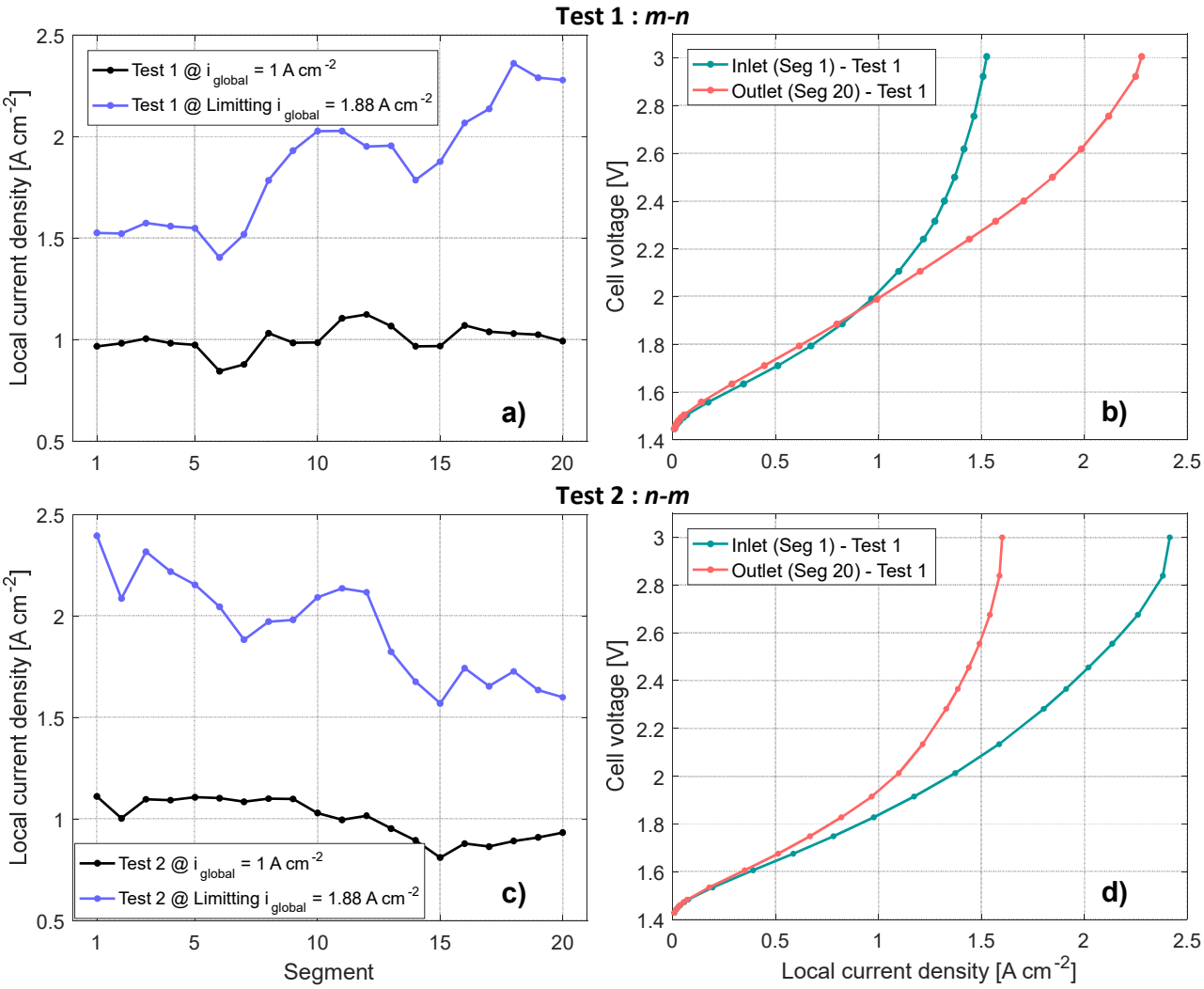

Figure 11. a) & c) Current densities profiles recorded during Test 1 (orientation m-n) and Test 2 (n-m) and b) & d) Local polarization curves recorded during Test 1 (m-n) and Test 2 (n-m)

Test 2 (orientation n-m):

For this test, the orientation of the PTL-VS was switched: the end "m" was placed at the outlet and the end "n" was placed at the inlet of the electrolyzer. Figure 11c shows the current density profile when the global limiting current density is reached, and Figure 11d presents the local polarization curves for the Segments 1 and 20. It was found that the behavior was reversed with respect to the first test, i.e., for this new orientation of the PTL-VS, the local limiting current density was lower at the outlet than at the inlet of the cell. Hence, the transport limitations were more important in the outlet zone, as shown by the local polarization curves.

In order to have more insights, the PTL-VS was cut into 20 pieces of 1.5 x 1 cm^2, corresponding to each segment of the electrolysis cell. Then, the permeability of each segment was calculated by measuring the loss of charge and plotted in Figure 12. In this figure, the segment 1 (inlet) represents the end "m" and the segment 20 (outlet) represents the end "n". These measurements revealed that the PTL-VS properties were not homogenous.

For instance, the permeability progressively increases between the inlet and outlet, going from around $0.8x10^{-14}$ to $1.6x10^{-14}$ m^2. Then, the heterogeneous current density distribution that was observed when transport limitations appeared is in agreement with the change of permeability of the PTL. In fact, comparing against the outlet, the lower permeability in the inlet zone indicates a lower capability to transport the gas/water through the PTL-VS.

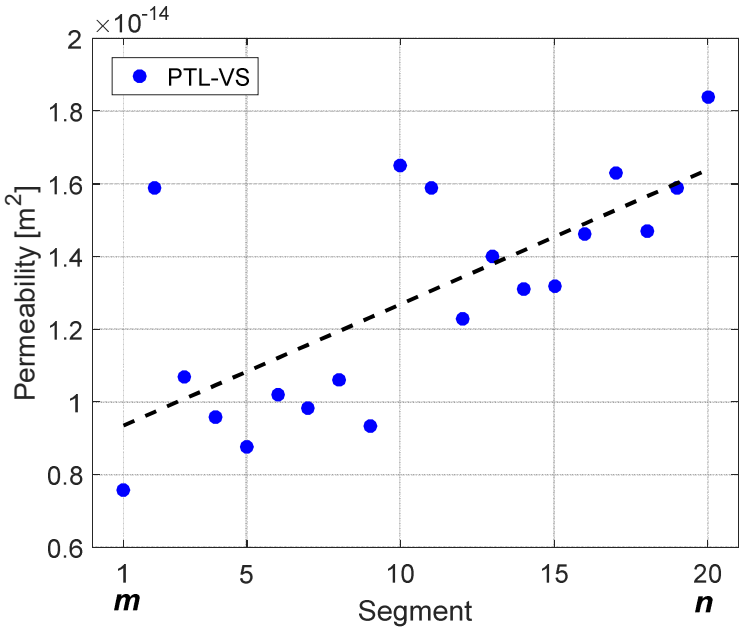

Figure 12 PTL-VS local permeability – Results are presented according to the orientation segment 1: m and segment 20: n

Therefore, it can be concluded that the current density heterogeneities, when transport limitations appeared, were mainly a consequence of the changes in PTL-VS properties, which are inherent to the fabrication process.

Furthermore, this suggests that the heterogeneous nature of the porous media used in industrial electrolyzer can play a fundamental role in their performance and current density distribution.

4. Conclusions

Four different Titanium powder PTLs were compared based on characteristics such as mean pore size and porosity, and their influence on the electrolysis cell performance was studied. Better results were found for a PTL with a mean pore size around 10 µm and a porosity of 31%. The best performance was obtained thanks to a lower contact resistance with the catalyst layer, especially at high current densities, where the cell voltage was about 100 mV lower than the voltage obtained when using a PTL with a mean pore size around 60 µm and a porosity of 37%.

In addition, a model of the constriction resistance between the catalyst layer and the PTL was proposed. This model demonstrated the optimal pore size of the PTL not only depends on the working condition of the electrolyzer, but also on the thickness and the electrical conductivity of the catalyst layer.

Furthermore, gas/water transport limitations were obtained when using a PTL with a mean pore size around 3 µm. It was demonstrated that the increase of the operating pressure reduces the effects of the transport limitations and increases the limiting current density range since the pressure reduces the oxygen bubbles size, which facilitates their expelling and leaves more available space for the water arrival to the catalyst zone. Moreover, a local characterization of these problems was made using the segmented electrolysis cell. Hence, a heterogeneous distribution of the current density profile between the inlet and the outlet was found, which was caused by the changing properties of the PTL along the cell.

Acknowledgments

This study was supported by the French Environment and Energy Management Agency (ADEME) and the French Grand Est Region.

REFERENCES

[1] AIE. Renewables 2018 : Analysis and Forecasts to 2023. Paris: AIE; 2018. doi:10.1787/re_mar-2018-en.

[2] Hydrogen scaling up A sustainable pathway for the global energy transition. Hydrogen Council; 2017.

[3] Fouda-Onana F, Chandesris M, Médeau V, Chelghoum S, Thoby D, Guillet N. Investigation on the degradation of MEAs for PEM water electrolysers part I: Effects of testing conditions on MEA performances and membrane properties. Int J Hydrogen Energy 2016;41:16627–36. doi:10.1016/j.ijhydene.2016.07.125.

[4] Carmo M, Fritz DL, Mergel J, Stolten D. A comprehensive review on PEM water electrolysis. Int J Hydrogen Energy 2013;38:4901–34. doi:10.1016/j.ijhydene.2013.01.151.

[5] Buttler A, Spliethoff H. Current status of water electrolysis for energy storage, grid balancing and sector coupling via power-to-gas and power-to-liquids: A review. Renew Sustain Energy Rev 2018;82:2440–54. doi:10.1016/j.rser.2017.09.003.

[6] Espinosa-López M, Darras C, Poggi P, Glises R, Baucour P, Rakotondrainibe A, et al. Modelling and experimental validation of a 46 kW PEM high pressure water electrolyzer. Renew Energy 2018;119:160–73. doi:10.1016/j.renene.2017.11.081.

[7] Babic U, Suermann M, Büchi FN, Gubler L, Schmidt TJ. Critical Review—Identifying Critical Gaps for Polymer Electrolyte Water Electrolysis Development. J Electrochem Soc 2017;164:F387–99. doi:10.1149/2.1441704jes.

[8] Grigoriev SA, Kalinnikov AA, Millet P, Porembsky VI, Fateev VN. Mathematical modeling of high-pressure PEM water electrolysis. J Appl Electrochem 2010;40:921–32. doi:10.1007/s10800-009-0031-z.

[9] Suermann M, Schmidt TJ, Buchi FN. Investigation of Mass Transport Losses in Polymer Electrolyte Electrolysis Cells. ECS Trans 2015;69:1141–8. doi:10.1149/06917.1141ecst.

[10] Lee CH, Banerjee R, Arbabi F, Hinebaugh J, Bazylak A. Porous Transport Layer Related Mass Transport Losses in Polymer Electrolyte Membrane Electrolysis: A Review. ASME 2016 14th Int. Conf. Nanochannels, Microchannels, Minichannels, 2016, p. V001T07A003. doi:10.1115/ICNMM2016-7974.

[11] Millet P, Ranjbari A, De Guglielmo F, Grigoriev SA, Auprêtre F. Cell failure mechanisms in PEM water electrolyzers. Int J Hydrogen Energy 2012;37:17478–87. doi:10.1016/j.ijhydene.2012.06.017.

[12] Feng Q, Yuan XZ, Liu G, Wei B, Zhang Z, Li H, et al. A review of proton exchange membrane water electrolysis on degradation mechanisms and mitigation strategies. J Power Sources 2017;366:33–55. doi:10.1016/j.jpowsour.2017.09.006.

[13] Kaviany M. Principles of Heat Transfer in Porous Media. Springer New York; 2012.

[14] Grigoriev SA, Millet P, Volobuev SA, Fateev VN. Optimization of porous current collectors for PEM water electrolysers. Int J Hydrogen Energy 2009;34:4968–73. doi:10.1016/j.ijhydene.2008.11.056.

[15] Majasan JO, Iacoviello F, Shearing PR, Brett DJ. Effect of Microstructure of Porous Transport Layer on Performance in Polymer Electrolyte Membrane Water Electrolyser. Energy Procedia 2018;151:111–9. doi:10.1016/j.egypro.2018.09.035.

[16] Majasan JO, Iacoviello F, Cho JIS, Maier M, Lu X, Neville TP, et al. Correlative study of microstructure and performance for porous transport layers in polymer electrolyte membrane water electrolysers by X-ray computed tomography and electrochemical

characterization. Int J Hydrogen Energy 2019;44:19519–32. doi:10.1016/j.ijhydene.2019.05.222.
[17] Siracusano S, Di Blasi A, Baglio V, Brunaccini G, Briguglio N, Stassi A, et al. Optimization of components and assembling in a PEM electrolyzer stack. Int J Hydrogen Energy 2011;36:3333–9. doi:10.1016/j.ijhydene.2010.12.044.
[18] Li H, Fujigaya T, Nakajima H, Inada A, Ito K. Optimum structural properties for an anode current collector used in a polymer electrolyte membrane water electrolyzer operated at the boiling point of water. J Power Sources 2016;332:16–23. doi:10.1016/j.jpowsour.2016.09.086.
[19] Ito H, Maeda T, Nakano A, Kato A, Yoshida T. Influence of pore structural properties of current collectors on the performance of proton exchange membrane electrolyzer. Electrochim Acta 2013;100:242–8. doi:10.1016/j.electacta.2012.05.068.
[20] Ito H, Maeda T, Nakano A, Hwang CM, Ishida M, Kato A, et al. Experimental study on porous current collectors of PEM electrolyzers. Int J Hydrogen Energy 2012;37:7418–28. doi:10.1016/j.ijhydene.2012.01.095.
[21] Schuler T, Bruycker R De, Schmidt TJ, Buchi FN. Polymer electrolytewater electrolysis: Correlating porous transport layer structural properties and performance: Part i. tomographic analysis of morphology and topology. J Electrochem Soc 2019;166:F270–81. doi:10.1149/2.0561904jes.
[22] Schuler T, Schmidt TJ, Büchi FN. Polymer Electrolyte Water Electrolysis: Correlating Performance and Porous Transport Layer Structure: Part II. Electrochemical Performance Analysis. J Electrochem Soc 2019;166:F555–65. doi:10.1149/2.1241908jes.
[23] Han B, Mo J, Kang Z, Zhang FY. Effects of membrane electrode assembly properties on two-phase transport and performance in proton exchange membrane electrolyzer cells. Electrochim Acta 2016;188:317–26. doi:10.1016/j.electacta.2015.11.139.
[24] Han B, Mo J, Kang Z, Yang G, Barnhill W, Zhang FY. Modeling of two-phase transport in proton exchange membrane electrolyzer cells for hydrogen energy. Int J Hydrogen Energy 2017;42:4478–89. doi:10.1016/j.ijhydene.2016.12.103.
[25] Zinser A, Papakonstantinou G, Sundmacher K. Analysis of mass transport processes in the anodic porous transport layer in PEM water electrolysers. Int J Hydrogen Energy 2019;44:28077–87. doi:10.1016/j.ijhydene.2019.09.081.
[26] Lee JK, Lee CH, Bazylak A. Pore network modelling to enhance liquid water transport through porous transport layers for polymer electrolyte membrane electrolyzers. J Power Sources 2019;437:226910. doi:10.1016/j.jpowsour.2019.226910.
[27] Arbabi F, Montazeri H, Abouatallah R, Wang R, Bazylak A. Three-dimensional computational fluid dynamics modelling of oxygen bubble transport in polymer electrolyte membrane electrolyzer porous transport layers. J Electrochem Soc 2016;163:F3062–9. doi:10.1149/2.0091611jes.
[28] Ojong ET, Kwan JTH, Nouri-Khorasani A, Bonakdarpour A, Wilkinson DP, Smolinka T. Development of an experimentally validated semi-empirical fully-coupled performance model of a PEM electrolysis cell with a 3-D structured porous transport layer. Int J Hydrogen Energy 2017;42:25831–47. doi:10.1016/j.ijhydene.2017.08.183.
[29] Nouri-Khorasani A, Tabu Ojong E, Smolinka T, Wilkinson DP. Model of oxygen bubbles and performance impact in the porous transport layer of PEM water electrolysis cells. Int J Hydrogen Energy 2017;42:28665–80. doi:10.1016/j.ijhydene.2017.09.167.
[30] Lettenmeier P, Kolb S, Burggraf F, Gago AS, Friedrich KA. Towards developing a

backing layer for proton exchange membrane electrolyzers. J Power Sources 2016;311:153–8. doi:10.1016/j.jpowsour.2016.01.100.
[31] Lettenmeier P, Kolb S, Sata N, Fallisch A, Zielke L, Thiele S, et al. Comprehensive investigation of novel pore-graded gas diffusion layers for high-performance and cost-effective proton exchange membrane electrolyzers. Energy Environ Sci 2017;10:2521–33. doi:10.1039/c7ee01240c.
[32] Polonský J, Kodým R, Vágner P, Paidar M, Bensmann B, Bouzek K. Anodic microporous layer for polymer electrolyte membrane water electrolysers. J Appl Electrochem 2017;47:1137–46. doi:10.1007/s10800-017-1110-1.
[33] Kang Z, Yu S, Yang G, Li Y, Bender G, Pivovar BS, et al. Performance improvement of proton exchange membrane electrolyzer cells by introducing in-plane transport enhancement layers. Electrochim Acta 2019;316:43–51. doi:10.1016/j.electacta.2019.05.096.
[34] Liu C, Carmo M, Bender G, Everwand A, Lickert T, Young JL, et al. Performance enhancement of PEM electrolyzers through iridium-coated titanium porous transport layers. Electrochem Commun 2018;97:96–9. doi:10.1016/j.elecom.2018.10.021.
[35] Bessarabov D, Human G, Kruger AJ, Chiuta S, Modisha PM, du Preez SP, et al. South African hydrogen infrastructure (HySA infrastructure) for fuel cells and energy storage: Overview of a projects portfolio. Int J Hydrogen Energy 2017;42:13568–88. doi:10.1016/j.ijhydene.2016.12.140.
[36] Van Der Merwe J, Uren K, Van Schoor G, Bessarabov D. Characterisation tools development for PEM electrolysers. Int J Hydrogen Energy 2014;39:14212–21. doi:10.1016/j.ijhydene.2014.02.096.
[37] Verdin B, Fouda-Onana F, Germe S, Serre G, Jacques PA, Millet P. Operando current mapping on PEM water electrolysis cells. Influence of mechanical stress. Int J Hydrogen Energy 2017;42:25848–59. doi:10.1016/j.ijhydene.2017.08.189.
[38] Sun S, Xiao Y, Liang D, Shao Z, Yu H, Hou M, et al. Behaviors of a proton exchange membrane electrolyzer under water starvation. RSC Adv 2015;5:14506–13. doi:10.1039/c4ra14104k.
[39] Immerz C, Schweins M, Trinke P, Bensmann B, Paidar M, Bystroň T, et al. Experimental characterization of inhomogeneity in current density and temperature distribution along a single-channel PEM water electrolysis cell. Electrochim Acta 2018;260:582–8. doi:10.1016/j.electacta.2017.12.087.
[40] Immerz C, Bensmann B, Trinke P, Suermann M, Hanke-Rauschenbach R. Local current density and electrochemical impedance measurements within 50 cm single-channel PEM electrolysis cell. J Electrochem Soc 2018;165:F1292–9. doi:10.1149/2.0411816jes.
[41] Dedigama I, Angeli P, Van Dijk N, Millichamp J, Tsaoulidis D, Shearing PR, et al. Current density mapping and optical flow visualisation of a polymer electrolyte membrane water electrolyser. J Power Sources 2014;265:97–103. doi:10.1016/j.jpowsour.2014.04.120.
[42] Abbou S, Dillet J, Maranzana G, Didierjean S, Lottin O. Local potential evolutions during proton exchange membrane fuel cell operation with dead-ended anode – Part II: Aging mitigation strategies based on water management and nitrogen crossover. J Power Sources 2017;340:419–27. doi:10.1016/j.jpowsour.2016.10.045.
[43] Abbou S, Dillet J, Maranzana G, Didierjean S, Lottin O. Local potential evolutions during proton exchange membrane fuel cell operation with dead-ended anode – Part

I: Impact of water diffusion and nitrogen crossover. J Power Sources 2017;340:337–46. doi:10.1016/j.jpowsour.2016.11.079.
[44] Dullien FAL. Porous Media Fluid Transport and Pore Structure. Second Edi. San Diego: Academic Press; 1992. doi:https://doi.org/10.1016/B978-0-12-223651-8.50008-0.